MODELING OF PARTICLES INJECTED INTO A D.C. PLASMA JET

Y.C. Lee, K.C. Hsu and E. Pfender
Heat Transfer Division, Department of Mechanical Engineering,
University of Minnesota, Minneapolis, Minnesota 55455

ABSTRACT

A numerical study has been conducted for calculating the trajectories and phase change histories of particles injected into a confined D.C. thermal argon plasma jet. Necessary modifications of drag and heat transfer coefficients, and the coupling effects between injected particles and the plasma jet environment are taken into account. The mass reduction rate of the particles due to evaporation is used as the criterion for judging the performance of the plasma reactor.

1. INTRODUCTION

The interaction of particulate matter with thermal plasmas plays a key role in thermal plasma processing as, for example, in thermal plasma synthesis and reduction, in plasma spheroidization, in plasma spraying, etc. In spite of increasing efforts over the past years, our knowledge of the interaction of injected particles with plasmas is still incomplete.

Boulos (1) and Boulos and Gauvin (2), proposed a model for the motion and heating of particles in thermal RF plasmas. Yoshida and Akashi (3), as well as Fiszdon (4), considered a more detailed analysis of the heat transfer problem of particles exposed to thermal plasmas. Recently, Sayegh and Gauvin (5) used numerical techniques to determine the effect of strongly varying properties on the heat transfer coefficient between a plasma and a spherical particle. The relatively narrow temperature range (up to 5000 K), and the unrealistic negative drag coefficients require an extension of this work.

This paper considers the injection of fine powders into a confined thermal plasma jet. As a first step, the temperature and flow fields in the plasma jet are calculated based on a plasma reactor operated in this laboratory (6). After establishing the conditions in the plasma jet, the trajectories and temperature histories of particles injected into the plasma jet are calculated based on separately determined drag and heat transfer coefficients.

In view of thermal plasma synthesis, the mass reduction or particle evaporation rate is used as a criterion for the performance of a plasma reactor.

2. THE PLASMA JET

In this study a typical thermal plasma reactor is considered, operated with a D.C. plasma torch. The plasma jet emanating from the torch anode is confined in a reaction tube consisting of a refractory material. The particles are injected perpendicular to the axis of the plasma jet through a circumferential slot downstream, but close to the anode. In this way, the problem remains two-dimensional.

Figure 1 shows the control volume used as calculation domain. The governing equations are:

$$\text{continuity: } \frac{\partial}{\partial x}(\rho u_x) + \frac{1}{r}\frac{\partial}{\partial r}(\rho r u_r) = 0 \qquad (1)$$

momentum:

$$\rho u_x \frac{\partial u_x}{\partial x} + \rho u_r \frac{\partial u_x}{\partial r} = -\frac{\partial p}{\partial x} + 2\frac{\partial}{\partial x}\left(\mu \frac{\partial u_x}{\partial x}\right) + \frac{1}{r}\frac{\partial}{\partial r}\left(\mu r \frac{\partial u_x}{\partial r}\right) + \frac{1}{r}\frac{\partial}{\partial r}\left(\mu r \frac{\partial u_r}{\partial x}\right) \qquad (2)$$

$$\rho u_x \frac{\partial u_r}{\partial x} + \rho u_r \frac{\partial u_r}{\partial r} = -\frac{\partial p}{\partial r} + \frac{\partial}{\partial x}\left(\mu \frac{\partial u_r}{\partial x}\right) + \frac{2}{r}\frac{\partial}{\partial r}\left(\mu r \frac{\partial u_r}{\partial r}\right) + \frac{\partial}{\partial x}\left(\mu \frac{\partial u_x}{\partial r}\right) - \frac{2\mu u_r}{r^2} \qquad (3)$$

$$\text{energy: } \rho u_x \frac{\partial h}{\partial x} + \rho u_r \frac{\partial h}{\partial r} = \frac{\partial}{\partial x}\left(\frac{k}{C_p}\frac{\partial h}{\partial x}\right) + \frac{1}{r}\frac{\partial}{\partial r}\left(\frac{kr}{C_p}\frac{\partial h}{\partial r}\right) - S \qquad (4)$$

In these equations ρ represents the mass density, u the velocity, μ the viscosity, h the enthalpy, k the thermal conductivity, C_p the specific heat at constant pressure, and S the radiation losses (optically thin). In the case of multiple particle injection (Section 5), S includes the "heat sink effect" due to the injected solid material. The boundary conditions (Figure 1) are as follows:

A-B: $u_x = u_x$ derived from experiments (6)

$u_r = 0$

$h = h$ derived from experiments (6)

B-C and D-E: $u_x = 0$, $u_r = 0$, $h = h_{wall}$

C-D: $u_x = 0$, $u_r = v_{injection}$, $h = h_{wall}$

A-F: $\frac{\partial u_x}{\partial r} = 0$, $\frac{\partial u_r}{\partial r} = 0$, $\frac{\partial h}{\partial r} = 0$

E-F: $\frac{\partial u_x}{\partial x} = 0$, $u_r = 0$, $\frac{\partial h}{\partial x} = 0$ (fully developed)

The equations are solved by using a general purpose two-dimensional computer program, which is discussed in (7). The results of these calculations will be discussed together with the other results.

3. DRAG AND HEAT TRANSFER COEFFICIENTS

Drag and heat transfer coefficients are the two most important basic parameters needed for calculating trajectories and heat transfer for the injected particles. Lewis and Gauvin (8), Fiszdon (4), and Sayegh and Gauvin (5) suggest some correction factors for establishing the equations for these two coefficients.

Their suggestions are pertinent for plasma temperatures below 5,000 K. But, in the case of higher temperatures, the errors increase rapidly as the ionization increases which strongly affects viscosity, specific heat and thermal conductivity.

For a better understanding of these effects, an axisymmetric flow over a sphere with strongly variable properties is considered. Flow conditions range from Re $\doteq$ 0.1-50, free stream temperatures vary from T_∞ = 4,000 to 12,000 K, and the surface temperature of the sphere varies from T_w = 1,000 to 3,000 K. Assumptions and control volume are the same as used by Sayegh and Gauvin (5). The approach adopted in this work, however, makes use of the velocity equations instead of the vorticity stream function equations, and a much finer grid is employed close to the sphere in the near surface region.

Results are shown in Table 1 and 2. After data correlation, the following correction factors are obtained:

$$Nu_D = Nu_{D_f} \cdot \left(\frac{\rho_\infty \mu_\infty}{\rho_w \mu_w}\right)^{0.6} \left(\frac{C_{p\infty}}{C_{pw}}\right)^{0.38} \qquad (5)$$

$$C_{D\infty} = C_{D\infty_f} \cdot \left(\frac{\rho_\infty \mu_\infty}{\rho_w \mu_w}\right)^{-0.45} \qquad (6)$$

where $Nu_{D_f} = 2.0 + 0.60\ Re_f^{1/2}\ Pr_f^{1/3}$ (Ref. 9)

$$C_{D\infty_f} = \frac{24}{Re_f} + \frac{6.0}{1 + \sqrt{Re_f}} + 0.4 \quad \text{(Ref. 10)}$$

f: properties corresponding to the film temperature.
∞: properties corresponding to the free stream temperature.
w: properties corresponding to the sphere surface temperature.

$Nu_D = \frac{hD}{k}$

$C_{D\infty} = \frac{\text{Drag Force}}{\frac{\pi D^2}{4} \cdot \frac{1}{2}\rho u_\infty^2}$

These correction factors for establishing correlations valid for higher plasma temperatures represent an extention of constant property flow and for lower plasma temperatures. These factors will be used for calculations in the next section.

4. SINGLE PARTICLE INJECTION

For the case of a single particle injected into a D.C. plasma jet, we need to know the trajectory and the temperature variation of the particle in order to understand what happens within the jet.

The trajectory can be calculated by using the equation of motion considering viscous drag and inertia:

$$\vec{F}_1 = m\vec{a} = C_D \cdot \frac{\pi D^2}{4} \cdot 1/2\rho |\vec{u}_{relative}| \vec{u}_{relative} \qquad (7)$$

In addition, thermophoresis may be important under certain conditions. Accordingly, this effect is taken into account (11):

For $\lambda/R \leq 1$:

$$\vec{F}_2 = -18\pi \frac{\mu^2}{\rho T} R \left(\frac{1}{1+2C_m \frac{\lambda}{R}} \right) \left(\frac{\frac{K_g}{K_p} + C_t \frac{\lambda}{R}}{1+2\frac{K_g}{K_p} + 2C_t \frac{\lambda}{R}} \right) \nabla T_\infty \qquad (8)$$

For $\lambda/R > 1$:

$$\vec{F}_2 = -\frac{45}{64} \pi^2 \mu R u_\infty \lambda \cdot \frac{\nabla T_\infty}{T_\infty} \qquad (9)$$

where K_g, K_p are the thermal conductivities of the gas and of a particle, respectively, R is the radius of a particle, λ is the mean free path length of the gas molecules, and C_m, C_t are the correction factors (C_m = 1.13, C_t = 2.16 for the present situation).

At the same time, the heat transfer problem has to be solved within the particle, as well as between the particle and the plasma jet. Following the same method as employed by Fiszdon (4), but using fixed liquid-solid interface temperatures equal to the melting temperature, the moving boundary phase change problem can be solved. At the liquid-solid interface an artificial temperature difference equation is established which fixes $T_i = T_{melt}$ at this interface.

$$T_{i+1} + 10^{30} T_i + T_{i-1} - 10^{30} T_{melt} = 0$$

where i is the grid point at the interface.

Figure 2 shows the behavior of Alumina particles of different diameters with different injection velocities. Particles will reach the hottest zone (the central region in the plasma jet) if their diameter is approximately D = 20 µm and if their velocity is in the range from 20-30 m/s. This, however does not mean that this particle will have the best evaporation performance.

The calculations show that thermophoresis is important in the region near the wall where the temperature gradients reach

values up to 10^7 K/m. This force is then of the same order of magnitude as the viscous force (in the region 4/5 of the radius from the center line).

5. MULTI-PARTICLE INJECTION

In the following an actual powder injection process (multi-particle injection) will be considered assuming

(a) no particle-particle interaction,
(b) the initial particle size distribution and the injection velocity distribution are known,
(c) gas-particle interaction occurs only via energy transfer.

Based on these assumptions, the governing equations have been solved by the same method as described in section 4, taking the modified plasma jet environment due to heat sink effects into account (heat source term of equation (4)).

As an example, Alumina powder is considered with a size distribution and injection velocity distribution as listed in Table 3.

Figure 3, 4, and 5 show comparisons of the temperature fields between no-injection, carrier gas injection only, and multiple particle injection with carrier gas. Figure 3 shows the undisturbed temperature distribution of the plasma jet in the reactor tube and Figure 4 indicates the environment for single particle injection. A comparison of these two figures reveals that the injected gas which does not penetrate into the core of the plasma jet (12) has a "heat transfer shielding effect" on the plasma jet, i.e. the isotherms in Figure 4 extend somewhat farther downstream than without gas injection. The injected gas forms a gas shroud around the plasma jet reducing the relative velocity and, therefore, the convective heat transfer between plasma jet core and the surrounding gas.

Figure 5 illustrates the situation with multiple particle injection. A comparison with Figure 4 clearly demonstrates the "heat sink effect" of the injected particles. This influence on the plasma jet will increase as the injection load increases and in extreme situations of very high mass injection, the plasma jet would be quenched.

For judging the performance of a plasma reactor, the mass reduction rate (by evaporation) is introduced as a criterion in connection with synthesis in thermal plasmas. Results for the two cases listed in Table 3 are plotted in Figure 6 indicating a better performance for case 1 with 20 m/s mean injection velocity. The higher injection velocity in case 2 (30 m/s) reduces the dwell time of the particles in the hot core and reduces the total evaporation.

6. CONCLUSIONS

A numerical analysis for the injection of particles in a D.C. plasma jet leads to the following conclusions:

(a) Drag and heat transfer coefficients for a plasma flowing over a sphere require corrections as suggested by equations (5) and (6).
(b) Thermophoresis is important in regions close to the wall.

(c) The moving boundary phase change problem can be solved easily by fixing the melting temperature at the interface between solid and liquid phase.
(d) The mass reduction rate is a good indication for judging the performance of a plasma reactor for plasma synthesis.
(e) A specific example (Argon D.C. plasma jet with I=900 A, $\dot{m}_B$=0.51 g/s, $\dot{m}_I$=0.28 g/s) reveals that Alumina particles in the size range from 10-20 μm and 20 m/s mean injection velocity show the highest evaporation rate.

7. ACKNOWLEDGEMENT

This work has been supported by the National Science Foundation under grant NSF/CPE-7810047.

REFERENCES

(1) M.I. Boulos, IEEE TPS, PS-6, 93 (1978).

(2) M.I. Boulos and W.H. Gauvin, Can. J. Chem. Eng., 52, 355 (1974).

(3) T. Yoshida and K. Akashi, J. Appl. Phys., 48, 2252 (1977).

(4) J.K. Fiszdon, Int. J. Heat Mass Transfer, 22, 749 (1979).

(5) N.N. Sayegh and W.H. Gauvin, AIChE J., 25, 522 (1979).

(6) C. Boffa and E. Pfender, "Enthalpy Probe and Spectrometric Studies in an Argon Plasma Jet", HTLTR No. 73, Univ. of Minnesota, 1968.

(7) S.V. Patankar, Numerical Heat Transfer and Fluid Flow, Hemisphere Publishing Corporation, 1980.

(8) J.A. Lewis and W.H. Gauvin, AIChE, 19, 982 (1973).

(9) W.E. Ranz and W.R. Marshall, Jr., Chem. Eng. Progress, 48, 173 (1952).

(10) F.M. White, Viscous Fluid Flow, McGraw Hill Book Co., 1974.

(11) B.V. Derjaguin and Yu. I. Yalamov, "The Theory of Thermophroesis and Diffusiophoresis of Aerosol Particles and Their Experimental Testing", in Topics in Current Aerosol Research, edited by G.M. Hidy and T.R. Brock, Pergamon Press, 1972.

(12) D.M. Chen, K.C. Hsu, C.H. Liu and E. Pfender, IEEE, TPS, PS-8, 425 (1980).

Table 1: Heat Transfer Coefficients (Nu_∞)

Re_∞ \ $T_\infty - T_w$	Constant Properties		4,000 -1,000K	10,000 -2,500K	12,000 -3,000K
	Semi-Empirical Correlation	Calculated*			
0.1	2.17	2.08	1.23	0.73	0.59
1.0	2.52	2.19	1.55	0.83	0.68
10.0	3.65	3.29	2.60	1.34	1.20
20.0	4.34	3.96	3.29	1.68	1.40
50.0	5.70	5.29	4.66	2.27	1.67

*based on 4,000K

$$Re_\infty = \frac{\rho_\infty u_\infty D}{\mu_\infty} \qquad Nu_\infty = \frac{hD}{K_\infty}$$

Semi-empirical correlation (Ref. 9):

$$Nu = 2. + 0.6\, Re^{1/2} Pr^{1/3}$$

Table 2: Drag Coefficients

Re_∞ \ $T_\infty - T_w$	Constant Properties		4,000 -1,000K	10,000 -2,500K	12,000 -3,000K
	Semi-Empirical Correlation	Calculated*			
0.1	245.0	252.1	100.8	151.9	199.9
1.0	27.4	24.4	15.4	17.6	22.4
10.0	4.2	4.3	2.9	3.3	4.2
20.0	2.7	2.6	1.8	2.1	2.6
50.0	1.6	1.4	1.0	1.2	1.4

*based on 4,000K

$$Re_\infty = \frac{\rho_\infty u_\infty D}{\mu_\infty}$$

$$C_D = \frac{\text{Force}}{\frac{\pi D^2}{4} \cdot \frac{1}{2} \rho_\infty u_\infty^2}$$

Semi-empirical correlation (Ref. 10):

$$C_D = \frac{24}{Re} + \frac{6}{1 + \sqrt{Re}} + 0.4$$

Table 3: Multi-particle Injection
(total mass of injected particles= 6×10^{-3} g/s)

Case	Particle Size Distribution		Injection Velocity Distribution	
	Diameter (μm)	Weighting Function	Velocity(m/s)	Weighting Function
Case 1	10	0.25	15	0.25
	15	0.50	20	0.50
	20	0.25	25	0.25
Case 2	10	0.25	25	0.25
	15	0.50	30	0.50
	20	0.25	35	0.25

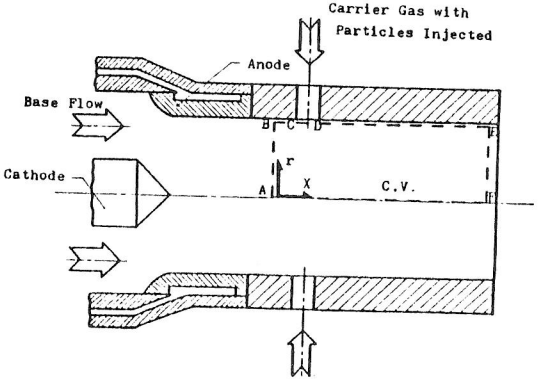

Fig. 1: Schematic Diagram of a D.C. Plasma Jet.

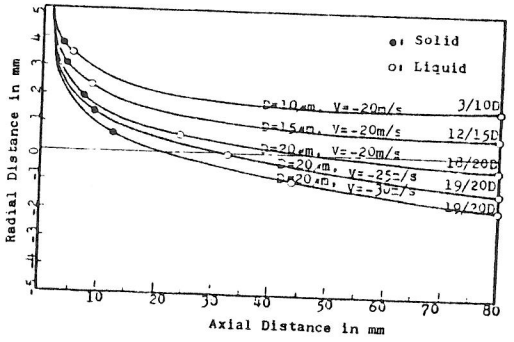

Fig. 2: Trajectories of Particles Injected into a D.C. Argon Plasma Jet.

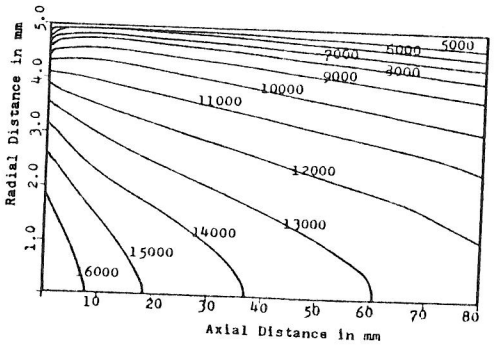

Fig. 3: Temperature Field of a D.C. Argon Plasma Jet (I=900A, Base Flow=0.51 g/s, No Carrier Gas, No Particles Injected).

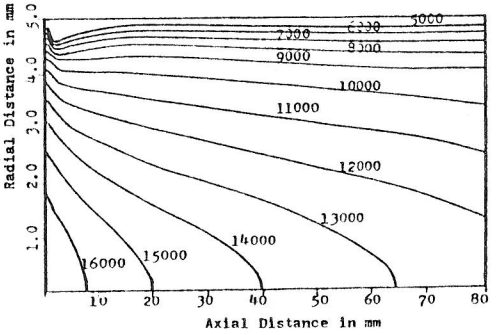

Fig. 4: Temperature Field of a D.C. Argon Plasma Jet (I=900A, Base Flow=0.51 g/s, Carrier Gas=0.28 g/s, No Particles Injected)

Fig. 5: Temperature Field of a D.C. Argon Plasma Jet (I=900A, Base Flow=0.51 g/s, Carrier Gas=0.28 g/s, Particles Injected=0.006 g/s).

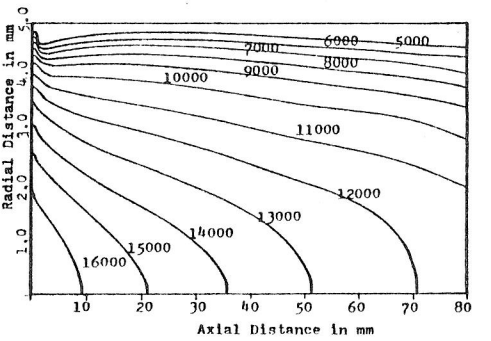

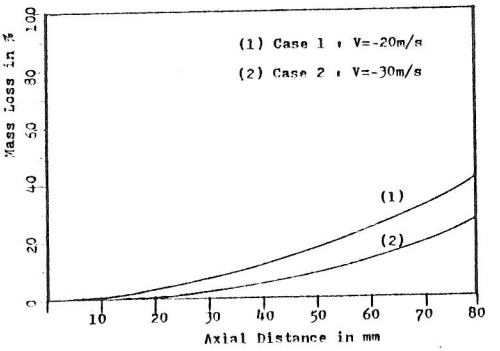

Fig. 6: Mass Reduction Rates of Particles Injected into a D.C. Argon Plasma Jet.